International Journal of Heat and Fluid Flow 31 (2010) 57–69

Contents lists available at ScienceDirect

International Journal of Heat and Fluid Flow

journal homepage: www.elsevier.com/locate/ijhff

Analysis of thermal dispersion in an array of parallel plates with fully-developed laminar flow

Jiaying Xu [a], Tian-Jian Lu [b], Howard P. Hodson [a], Norman A. Fleck [a,*]

[a] Department of Engineering, University of Cambridge, Trumpington Street, Cambridge CB2 1PZ, UK
[b] SV Laboratory, School of Aerospace, Xi'an Jiaotong University, Xi'an, Shaanxi Province 710049, PR China

ARTICLE INFO

Article history:
Received 30 June 2008
Received in revised form 13 September 2009
Accepted 9 October 2009
Available online 6 December 2009

Keywords:
Thermal dispersion
Parallel-plate array
Fully-developed laminar flow
Peclet number

ABSTRACT

The effect of thermal dispersion upon heat transfer across a periodic array of parallel plates is studied. Three basic heat transfer problems are addressed, each for steady, fully-developed, laminar fluid flow: (a) transient heat transfer due to an arbitrary initial temperature distribution within the fluid, (b) steady heat transfer with constant heat flux on all plate surfaces, and (c) steady heat transfer with constant wall temperatures. For problems (a) and (b), the effective thermal dispersivity scales with the Peclet number Pe according to $1 + CPe^2$, where the coefficient C is independent of Pe. For problem (c) the coefficient C is a function of Pe.

1. Introduction

Mass and heat convective transport processes in multiphase systems (e.g., packed beds, cellular foams, lattice materials) are of considerable practical importance as they occur in compact heat exchangers, chemical reactions, groundwater movements, food manufacturing and storage, heat carrying and cooling in nuclear power stations, and so on. However, apart from a few idealized models, detailed fluid flow and heat transfer at the pore level in these porous media are complicated and difficult to analyse, owing to the complex microstructure. Therefore, with focus placed on the overall aspects of mass, momentum, and energy conservation principles, volume-averaged quantities are commonly used to simplify the analysis.

Much effort has been expended in calculating the effective thermal properties of a fluid-saturated porous medium, such as its effective conductivity and effective diffusivity. The rule-of-mixtures approximation is frequently adequate when the fluid is motionless. When the fluid is moving, an additional effective thermal property of the porous media becomes relevant, namely, the *effective thermal dispersivity* (Taylor, 1953, 1954; Aris, 1956; Kurzweg and Jaeger, 1997; Yuan et al., 1991; Batycky et al., 1993; Kuwahara et al., 1996, 2001; Kuwahara and Nakayama, 1999; Nakayama and Kuwahara, 1999; Quintard et al., 1997; Zanotti and Carbonell, 1984a–c; Xu, 2006; Quintard and Whitaker, 1993). Thermal dispersion is due to the combined effects of heat diffusion in both the fluid and solid and to thermal convection within the fluid.

The applicability of an effective thermal dispersivity is not restricted to convective heat transfer in porous media. For example, the concept of an effective dispersivity is useful for the analysis of heat transfer in thermally conducting fluids moving past a thermally conducting solid phase, e.g., thermal pulse propagation in laminar flow within small diameter tubes (conduits) Kurzweg and Jaeger, 1997; Yuan et al., 1991. These mathematically rigorous studies, based on idealized geometries, are useful for understanding the fundamental mechanism of thermal dispersion across porous media such as packed beds. For example, Carbonell and colleagues (1984a–c) have made use of idealized porous medium models in order to obtain the dispersion–convection characteristics of temperature variations in flows through packed beds; their models have been widely made use of in chemical engineering applications (Kurzweg and Jaeger, 1997).

The concept of dispersion was first developed for the analysis of mass transfer in porous media (Taylor, 1953, 1954; Aris, 1956). Velocity variations within a porous microstructure enhance the mixing of fluid flow, and thereby speed up the spreading of mass components from high concentration to low. In the analysis of mass dispersion, the focus is shifted from length scales on the order of the pores (i.e., the microscopic level) to the volume-averaged (macroscopic) level. As a result of the averaging process, an effective dispersivity appears naturally in the governing equations. The mathematics of thermal dispersion is the same as for mass

* Corresponding author. Tel.: +44 01223 748240; fax: +44 01223 332662.
E-mail address: NAF1@cam.ac.uk (N.A. Fleck).

0142-727X/$ - see front matter Crown Copyright © 2009 Published by Elsevier Inc. All rights reserved.
doi:10.1016/j.ijheatfluidflow.2009.10.003

Nomenclature

c_p	specific heat capacity under constant pressure, J kg^{-1} K^{-1}
D	half-height of cell containing fluid and plate, m
H	half-height of unit fluid channel, m
h	effective heat transfer coefficient between plate surface and the bulk fluid, W m^{-2} K^{-1}
L	length of plate array, m
Nu	Nusselt number, $Nu = \frac{h2H}{\lambda_f}$
Pe	Peclet number, $Pe = \frac{u_m 2H}{a_f} = \frac{u_{av} 2D}{a_f}$
Pr	Prandtl number, $Pr = \frac{\nu_f}{a_f} = \frac{Pe}{Re}$
$\dot{Q}$	heat source density in solid plates, W/m^3
q	heat flux, W m^2
Re	Reynolds number, $Re = \frac{u_m 2H}{\nu_f} = \frac{u_{av} 2D}{\nu_f}$
T	temperature, K
t	time, s
u	fluid velocity, m s^{-1}
x, y, z	Cartesian coordinates, m

Greek letters

α	thermal diffusivity, $\alpha = \frac{\lambda}{\rho c_p}$, m^2 s^{-1}
β	ratio of solid-to-fluid molecular conductivity, $\beta = \lambda_s/\lambda_f$
λ	thermal conductivity, W m^{-1} K^{-1}
ε	structural porosity, $\varepsilon = \frac{H}{D}$
η	dimensionless space coordinate in y-direction, $\eta = \frac{y}{H}$
θ	dimensionless temperature
μ	molecular viscosity, kg m^{-1} s^{-1}
ν	kinetic viscosity, m^2 s^{-1}
ξ	dimensionless space coordinate in x-direction, $\xi = \frac{x}{L}$
ρ	density, kg m^{-3}
σ	ratio of two length scales, $\sigma = \frac{H}{L}$
Φ	generic variable
φ	ratio of solid-to-fluid thermal diffusivity, $\phi = \alpha_s/\alpha_f$
ω_1	dimensionless time coordinate for convection, $\omega_1 = \frac{u_m t}{L}$
ω_2	dimensionless time coordinate for diffusion, $\omega_2 = \frac{a_f t}{L^2}$

Subscripts

f	fluid
s	solid
eff	effective
av	volume average
m	bulk-mean

dispersion, with concentration replaced by temperature. The effective thermal dispersivity is affected by the presence of porosity and flow parameters in addition to the constituent materials; it is the key parameter for dispersion analysis in porous media at the macroscopic level.

Porous media such as packed beds, cellular foams and lattice materials have complex micro-architectures, making difficult an accurate evaluation of the effective dispersivity of temperature or mass. To simplify the geometry, idealized geometries are commonly used to represent the porous media, for example an array of parallel plates or circular tubes (Kurzweg and Jaeger, 1997; Yuan et al., 1991), or periodically arranged spheres or rods (Kuwahara et al., 1996; Kuwahara and Nakayama, 1999). After volume-averaging, there is no essential difference between the macroscopic response of these idealized models and that of the more realistic porous structures. The advantage of using idealized models is that analytical solutions at the pore level can be obtained and lead to macroscopic effective constitutive relations that guide the dispersion analysis of porous media having more complicated structures. For example, Taylor (1953) studied the transient dispersion of mass along a circular tube, and the results show that the effective dispersivity is a function of flow Peclet number only.

Several attempts have been made to analyse thermal dispersion in simple porous media. For example, Kurzweg and Jaeger (1997) studied the transient response due to an initial temperature distribution in the fluid, using an array of parallel plates of zero thickness, and thereby obtained the effective thermal dispersion conductivity. Yuan et al. (1991) analytically studied thermal dispersion using thick-walled tubes, for both transient and steady heat transfer, and obtained asymptotic solutions. They found that the non-dimensional dispersive term has the form of $1 + CPe^2$, where the Peclet number Pe can be expressed in terms of the Prandtl number Pr and the Reynolds number Re according to $Pe = PrRe$. The proportionality coefficient C depends upon the aspect ratio of tube cross-section, upon the thermal properties of fluid and tube, and upon the temperature field. Batycky et al. (1993) used the Taylor expansion technique to study thermal dispersion in a circular cylinder and confirmed the Pe^2 dependence.

The above studies of thermal dispersion are based upon transient analyses where the temperature of the incoming fluid undergoes a step-wise change and the subsequent temperature field is determined as a function of space and time (while the underlying fluid flow is steady and generally considered laminar). The so-obtained thermal dispersivity is then applied to steady-state heat transfer in porous media (Kuwahara et al., 1996, 2001; Kuwahara and Nakayama, 1999; Nakayama and Kuwahara, 1999; Quintard et al., 1997), without justification. In order to validate whether the dispersion obtained in transient analysis can be applied for steady cases, the present study has assessed thermal dispersion in both transient and steady cases. For simplicity, a parallel-plate array serves as the prototypical porous medium, with fully-developed laminar fluid flow. Both transient and steady heat transfers are analysed. In the steady state analysis, the sensitivity of response to the choice of thermal boundary condition is addressed. In addition, the effect of porosity of the idealized porous medium upon thermal dispersivity is quantified.

2. Problem description

Consider steady-state laminar flow of an incompressible liquid through an array of equi-spaced parallel plates, as shown in Fig. 1a along with the coordinate system. We shall refer to the plate material as the solid phase and the moving liquid between the stationary plates as the fluid phase, and use superscripts and subscripts s and f to denote the solid and fluid, respectively. We assume that the plates are large in both the stream-wise x-direction and the span-wise z-direction, compared to the cross-flow y-direction, and also assume that the number of plates in the y-direction is large. The problem can then be considered as two-dimensional in the (x, y) plane; also, the flow is taken to be fully-developed, with entry and exit effects ignored. Periodicity in the y-direction allows for volume averaging, with the integration performed over a unit channel only, $-D \leqslant y \leqslant D$, where $2D$ is the height of the unit cell. The problem thereby reduces to pseudo-one-dimensional after volume averaging.

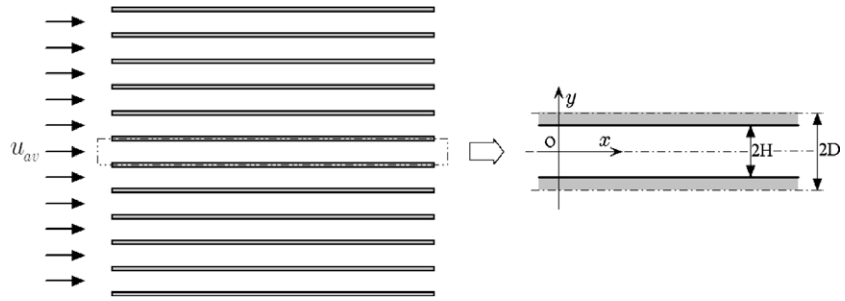

(a) The focused domain is taken from fully developed region

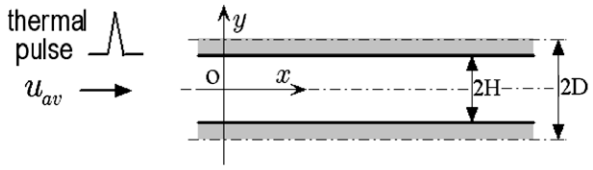

(b) Thermal pulse introduced to cause transient heat transfer

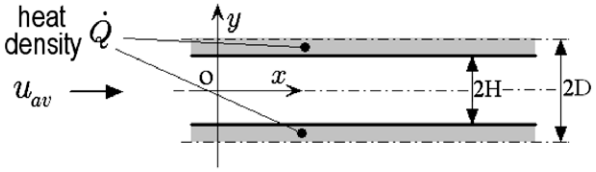

(c) Steady heat transfer with uniform-distributed heat source density within solid plates

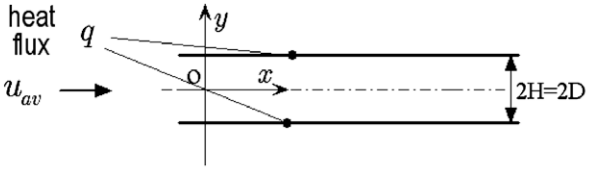

(d) Fixed heat flux along solid plates with zero-thickness

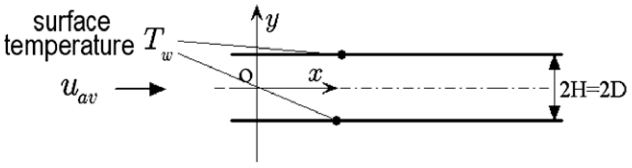

(e) Fixed surface temperature along solid plates with zero-thickness

Fig. 1. Parallel plate array model. (a) The domain of interest, (b) the case with transient heat transfer, (c) the case with steady-state heat transfer, with uniform-distributed heat source density within solid plates, (d) the case of steady heat transfer with zero-thickness plates and fixed heat flux condition (e) the case of steady heat transfer with zero thickness and fixed surface temperature condition.

Consider fully-developed incompressible laminar flow in a channel of width $2H$ with bulk-mean fluid velocity u_m, see Fig. 1a. Fluid flow occurs only in the stream-wise x-direction, and the fluid velocity u_f within a representative channel varies parabolically with distance y from the mid-plane of the channel according to:

$$u_f = \frac{3}{2}u_m\left(1-\frac{y^2}{H^2}\right) \quad \text{for } -H \leqslant y \leqslant H. \tag{1}$$

The average velocity for the whole array is $u_{av} = \varepsilon u_m$ since the solid plates are taken to be stationary, where $\varepsilon = H/D$ is the structural porosity, defined as the ratio of void volume to the overall volume.

In the following sections, we shall study both transient and steady heat transfer in the parallel plates and analyse the heat dispersion accordingly. For transient heat transfer study, we assume no heat sources, as shown in Fig. 1b, but introduce a small temperature disturbance at the entrance – as demonstrated in the following section the disturbance profile is not important. Alternatively, for the study of steady heat transfer, we maintain a fixed heat source density $\dot{Q}$ or a fixed temperature T_w in the plates (different in value from that in the fluid). For the case of a fixed heat source density, $\dot{Q}$ the plate surfaces have a constant heat flux $q = \frac{\dot{Q}(1-\varepsilon)}{(1-\varepsilon)\rho_s c_{ps}+\varepsilon\rho_f c_{pf}}$, see Fig. 1c. Note that the heat flux q is finite, but the density $\dot{Q}$ is singular for the limiting case of a zero-thickness plates, as shown in Fig. 1d. For the case of a fixed plate temperature, the plates of zero thickness have a temperature T_w, see Fig. 1e.

In all cases considered, ideal heat transfer is assumed at the solid–fluid interface. Write T_s as the temperature in the solid phase and T_f as the temperature in the fluid phase, then there is

neither a jump in temperature nor in heat flux at the plate surfaces, giving:

$$T_s|_{y=\pm H} = T_f|_{y=\pm H} \quad \text{and} \quad -\lambda_s \left.\frac{\partial T_s}{\partial y}\right|_{y=\pm H} = -\lambda_f \left.\frac{\partial T_f}{\partial y}\right|_{y=\pm H}. \tag{2}$$

Here, λ_f and λ_s are thermal conductivities for the fluid phase and solid phase, respectively.

The effective thermal dispersion is determined in terms of volume-averaged quantities. Introduce the operator $\langle\rangle$, absent a superscript s or f, to denote volume-averaging over both phases, as follows. y-direction averaging over one channel $-D < y < D$ is defined by:

$$\langle \Phi \rangle = \frac{1}{2D}\int_{-D}^{D} \Phi dy = \frac{1}{D}\int_{0}^{D} \Phi dy, \tag{3}$$

where Φ is any variable, such as velocity u or temperature T. For example, the average velocity of the fluid and solid is $u_{av} = \langle u \rangle$. The averaging procedure splits a variable into two parts, the averaged value and the perturbed value $\Phi = \langle \Phi \rangle + \Phi'$.

Averaging is also performed over each phase, and this is termed *intrinsic* volume averaging. Denote $\langle\rangle^s$ as the volume-average over the solid phase, and $\langle\rangle^f$ as the volume-average over the fluid phase, such that

$$\langle \Phi \rangle^s = \frac{1}{2(D-H)}\left(\int_{H}^{D} \Phi dy + \int_{-D}^{-H} \Phi dy\right) = \frac{1}{D-H}\int_{H}^{D} \Phi dy, \tag{4}$$

and

$$\langle \Phi \rangle^f = \frac{1}{2H}\int_{-H}^{H} \Phi dy = \frac{1}{H}\int_{0}^{H} \Phi dy, \tag{5}$$

Here, we have exploited the symmetry of flow with respect to the mid-plane $y = 0$.

Write Φ_f as the value of Φ within the fluid phase and assume compact support such that $\Phi_f = 0$ in the solid phase. Likewise, write Φ_s as the value of Φ within the solid phase and assume that $\Phi_s = 0$ in the fluid phase. Then, the intrinsic and overall volume-averaged variables are related by:

$$\langle \Phi_f \rangle^f = \frac{1}{\varepsilon}\langle \Phi_f \rangle, \tag{6}$$

$$\langle \Phi_s \rangle^s = \frac{1}{1-\varepsilon}\langle \Phi_s \rangle. \tag{7}$$

Note that $\langle \Phi_s \rangle^f = 0$ and $\langle \Phi_f \rangle^s = 0$. Additional features of volume-averaging are given in Appendix A.

As already discussed, the problem described in this section is one-dimensional along the x-direction after averaging over the y-direction. The macroscopic momentum equation reduces to $\langle u \rangle \equiv u_{av}$ for fully-developed flow. The stream-wise velocities and pressure gradient are taken to be independent of x. And, after cross-flow y-direction averaging, the macroscopic energy equation depends only upon x.

Focusing now upon the macroscopic, one-dimensional problem, we analyse the energy balance in a small volume δx in the flow direction over a small time interval δt, as illustrated in Fig. 2. First note, that $\langle T \rangle$ denotes the macroscopic, volume-averaged temperature. Write $(\rho c_p)_{eff}$ as the effective thermal capacity per unit volume and denote the effective thermal conductivity by $\lambda_{eff} = (\rho c_p)_{eff} \cdot \alpha_{eff}$, in terms of the effective thermal diffusivity. Then, the total energy increase is $2D \cdot (\rho c_p)_{eff} \cdot \frac{\partial \langle T \rangle}{\partial t} \cdot \delta x \cdot \delta t$. The net energy increase due to conduction and convection is $2D \cdot \lambda_{eff} \cdot \frac{\partial^2 \langle T \rangle}{\partial x^2} \cdot \delta x \cdot \delta t$ and $2D \cdot (\rho c_p)_{eff} \cdot u_{av} \frac{\partial \langle T \rangle}{\partial x} \cdot \delta x \cdot \delta t$, respectively. If there exists an uniformly distributed heat source density $\dot{Q}$ in the solid plates, then the energy increase due to the heat source is $2(D-H) \cdot \dot{Q} \cdot \delta x \cdot \delta t$.

In subsequent sections, the role of the effective thermal dispersivity and the underlying physical mechanisms of thermal dispersion are explored further by developing analytical solutions to several particular cases of the parallel-plate model with particular choices of boundary condition and initial condition.

3. Transient heat transfer across an array of parallel plates

Consider the case where a thermal disturbance occurs within the porous medium (with no heat source available). We specialize this to the problem where a thermal pulse is introduced at the entrance of the parallel-plate array, as illustrated in Fig. 1b. Thermal penetration into the system is faster due to velocity non-uniformity across the channel, compared with that of plug flow with a uniform velocity distribution. Zanotti and Carbonell (1984a–c) have shown that, after a sufficiently long time period, the thermal pulse will travel at the same speed in both phases.

3.1. Effective thermal dispersion

The microscopic governing equation for the temperature T_s in the solid phase and the temperature T_f in the fluid phase are

$$\frac{\partial T_s}{\partial t} = \alpha_s\left(\frac{\partial^2 T_s}{\partial x^2} + \frac{\partial^2 T_s}{\partial y^2}\right) \quad \text{for } H \leqslant |y| \leqslant D, \tag{8}$$

$$\frac{\partial T_f}{\partial t} + u_f \frac{\partial T_f}{\partial x} = \alpha_f\left(\frac{\partial^2 T_f}{\partial x^2} + \frac{\partial^2 T_f}{\partial y^2}\right) \quad \text{for } |y| \leqslant H, \tag{9}$$

where t is time, $\alpha = \frac{\lambda}{\rho c_p}$ is the thermal diffusivity, and ρ, c_p and λ are material density, specific heat under constant pressure and thermal conductivity, respectively.

We proceed to homogenize Eqs. (8) and (9) into a single one-equation model (Quintard and Whitaker, 1994; Moyne et al., 2000) at the macroscopic level by assuming local thermal equilibrium $\langle T \rangle^f = \langle T \rangle^s = \langle T \rangle$. The assumption of local thermal equilibrium is valid when the net energy transfer between fluid phase and solid phase is zero. The more general case of local thermal non-equilibrium $\langle T \rangle^f \neq \langle T \rangle^s$ exists when the flow is not thermally fully-developed at entrance, or where the thermal conductivity difference

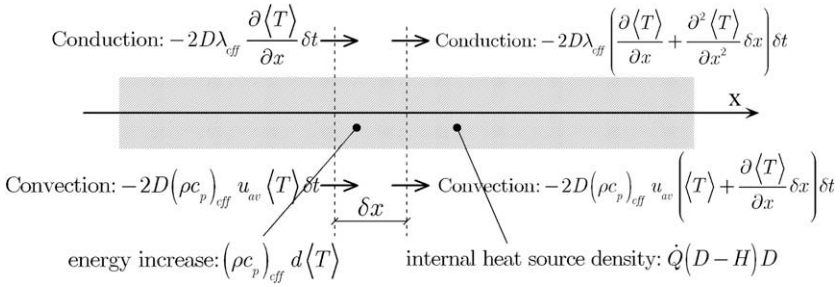

Fig. 2. One-dimensional energy balance analysis of the macroscopic representation.

between solid and fluid phases is extreme (Xu, 2006, pp. 30–31). A two-equation model is required for these cases (Quintard et al., 1997; Quintard and Whitaker, 1993; Hsiao and Advani, 1999). We emphasise that local thermal equilibrium is assumed herein.

We follow the theoretical work of Whitaker and his co-workers (1997, 1993, 1994, 1967) and Moyne et al. (2000), in order to evaluate the hydraulic dispersion effect. The energy equation after volume averaging can be written as:

$$\langle \rho c_p \rangle \frac{\partial \langle T \rangle}{\partial t} + \rho_f c_{pf} \frac{\partial \left(\langle u \rangle \langle T \rangle + \varepsilon \langle u_f' T_f' \rangle \right)}{\partial x} = \langle \lambda \rangle \frac{\partial^2 \langle T \rangle}{\partial x^2}, \tag{10}$$

where $\langle \rho c_p \rangle = [(1-\varepsilon)\rho_s c_{ps} + \varepsilon \rho_f c_{pf}]$ and $\langle \lambda \rangle = [(1-\varepsilon)\lambda_s + \varepsilon \lambda_f]$ are the volume-averaged heat capacity and thermal conductivity, respectively. Eq. (10) can be rephrased as:

$$\frac{\partial \langle T \rangle}{\partial t} + u_{av} \frac{\partial \langle T \rangle}{\partial x} = \langle \alpha \rangle \frac{\partial^2 \langle T \rangle}{\partial x^2} - \frac{\varepsilon \rho_f c_{pf}}{\langle \rho c_p \rangle} \frac{\partial \langle u_f' T_f' \rangle}{\partial x}, \tag{11}$$

where $\langle \alpha \rangle = \frac{\langle \lambda \rangle}{\langle \rho c_p \rangle}$ is the volume-averaged diffusivity.

On the right-hand side of Eq. (11), the first term expresses the contribution from thermal conduction and the second one accounts for dispersion. Upon combining these terms Eq. (11) reduces to

$$\frac{\partial \langle T \rangle}{\partial t} + u_{av} \frac{\partial \langle T \rangle}{\partial x} = \alpha_{eff} \frac{\partial^2 \langle T \rangle}{\partial x^2}, \tag{12}$$

where $\alpha_{eff} = \frac{\lambda_{eff}}{(\rho c_p)_{eff}}$ is the effective dispersivity and can be evaluated from:

$$\alpha_{eff} \frac{\partial \langle T \rangle}{\partial x} = \langle \alpha \rangle \frac{\partial \langle T \rangle}{\partial x} - \frac{\varepsilon \rho_f c_{pf}}{\langle \rho c_p \rangle} \langle u_f' T_f' \rangle, \tag{13}$$

or, in non-dimensional form,

$$\frac{\alpha_{eff}}{\langle \alpha \rangle} = 1 - \frac{\varepsilon \rho_f c_{pf}}{\langle \lambda \rangle} \frac{\langle u_f' T_f' \rangle}{\partial \langle T \rangle / \partial x} = 1 + \frac{\varepsilon \rho_f c_{pf}}{\langle \lambda \rangle} \frac{\langle u \rangle \langle T \rangle - \langle u_f T_f \rangle}{\partial \langle T \rangle / \partial x}. \tag{14}$$

The left-hand side of Eq. (14) is the relative effective thermal dispersivity. The number of unity on the right-hand side of Eq. (14) addresses the (relative) molecular diffusivity while the second term measures the pure dispersion effect. Thus, the above expression displays the feature that the effective diffusivity comprises both the molecular diffusivity and the dispersion effect.

In order to understand the physical meaning of thermal dispersion, we examine in more detail the second term on the right-hand side of Eq. (14). This contribution to dispersivity is inversely proportional to the heat flux density along the flow direction, $\langle \lambda \rangle \frac{\partial \langle T \rangle}{\partial x}$, and proportional to the difference between the uniformly distributed heat flux and the volume-averaged heat flux. As illustrated in Fig. 3, the uniformly distributed heat flux is contained within the vertical bar (shadowed region), whilst the volume-averaged heat flux is contained within the parabolic-shaped shadow area. The dispersion concept quantifies the microscopic non-uniformity of the heat flux distribution. There is no dispersion in a porous medium if either the velocity or temperature is uniformly distributed at the microscopic (pore) level. The non-uniformity of velocity distribution within each fluid channel is a consequence of the porous structure; the non-uniformity of temperature distribution is attributed to both the velocity non-uniformity and the thermal boundary conditions.

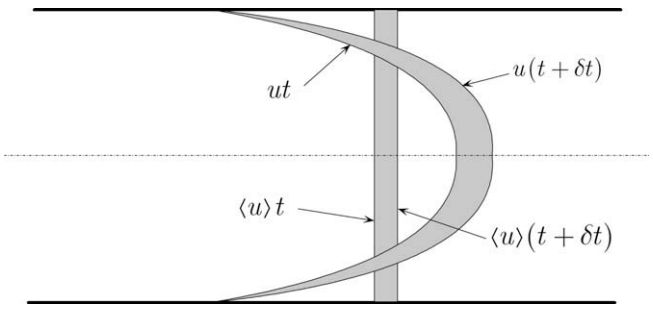

Fig. 3. Physical representations of heat fluxes: curved area: actual area containing heat flux for the averaging procedure. Vertical bar: assumingly uniformly distributed heat flux.

We proceed to evaluate Eq. (14). First, the spatial coordinates are non-dimensionalized as:

$$\xi = \frac{x}{L}; \quad \eta = \frac{y}{H}, \tag{15}$$

where the plate length L is a length scale at the structural level, and is usually much larger than the length scale at the pore level, i.e. $L \gg D \sim H$. The time coordinate is converted to two timescales:

$$\omega_1 = \frac{u_m t}{L}; \quad \omega_2 = \frac{\alpha_f t}{L^2}, \tag{16}$$

where ω_1 is the non-dimensional timescale associated with the stream-wise convection and ω_2 the one with the molecular diffusion. This kind of multiple time scale analysis is generally employed to deal with processes where fast and slow dynamics coexist (Vora et al., 2006; Mahecha-Botero et al., 2007). Application of the chain rule of differentiation with respect to time results in:

$$\frac{\partial \Phi}{\partial t} = \frac{\partial \Phi}{\partial \omega_1} \frac{d\omega_1}{dt} + \frac{\partial \Phi}{\partial \omega_2} \frac{d\omega_2}{dt} = \frac{u_m}{L} \frac{\partial \Phi}{\partial \omega_1} + \frac{\alpha_f}{L^2} \frac{\partial \Phi}{\partial \omega_2}.$$

The reasons to use two different length scales and two different time scales are:

(1) Heat transfer mechanisms in the x- and y-directions are different: heat transfer along the stream-wise x-direction is by both convection and conduction; in the cross-flow y-direction, only conduction occurs. With a slow flow, e.g., Peclet number (Pe, as described in the next paragraph) is smaller than 5, the x-direction conduction is relatively significant compared with the convection; as Peclet number increases, convection dominates over conduction.
(2) The speeds of heat penetration are different for convection and diffusion. The former is faster than the latter at a Peclet number greater than 1.
(3) Consequently, different physical phenomena will be separated in the governing equations by using different length and time scales.

We introduce some useful dimensionless parameters for later convenience: Reynolds number, $Re = \frac{u_{av} 2D}{\nu_f} = \frac{u_m 2H}{\nu_f}$; Prandtl number, $Pr = \frac{\nu_f}{\alpha_f} = \frac{\mu_f c_{pf}}{\lambda_f}$; Peclet number, $Pe = \frac{u_{av} 2D}{\alpha_f} = \frac{u_m 2H}{\alpha_f} = RePr$. Write h as the effective heat transfer coefficient between plate surface and the bulk fluid, $h = \frac{q}{T_w - T_m}$, where q is the heat flux from solid surface to fluid, T_w and T_m are the temperature values of the plate surface and bulk fluid, respectively. Then, the Nusselt number is $Nu = \frac{2Hh}{\lambda_f}$, where ν_f and μ_f are the kinematical and molecular fluid viscosity, with $\nu_f = \frac{\mu_f}{\rho_f}$.

The governing equations (8) and (9) are thereby non-dimensionalized to the form:

$$\frac{Pe}{2} \sigma \frac{\partial T_f}{\partial \omega_1} + \sigma^2 \frac{\partial T_f}{\partial \omega_2} + \frac{3Pe}{4} \sigma (1 - \eta^2) \frac{\partial T_f}{\partial \xi} = \sigma^2 \frac{\partial^2 T_f}{\partial \xi^2} + \frac{\partial^2 T_f}{\partial \eta^2} \quad \text{for } 0 \leqslant \eta \leqslant 1, \tag{17}$$

$$\frac{Pe}{2\phi}\sigma\frac{\partial T_s}{\partial\omega_1}+\frac{\sigma^2}{\phi}\frac{\partial T_s}{\partial\omega_2}=\sigma^2\frac{\partial^2 T_s}{\partial\xi^2}+\frac{\partial^2 T_s}{\partial\eta^2}\quad\text{for } 1\leqslant\eta\leqslant\frac{1}{\varepsilon},\tag{18}$$

where $\sigma=\frac{H}{L}$ and $\phi=\frac{\alpha_s}{\alpha_f}$. Similarly, the continuity of temperature and heat-flux boundary conditions (as described originally by Eq. (2)) become:

$$T_s|_{\eta=1}=T_f|_{\eta=1},\quad \left.\frac{\partial T_f}{\partial\eta}\right|_{\eta=1}=\beta\left.\frac{\partial T_s}{\partial\eta}\right|_{\eta=1},\tag{19}$$

for interfacial boundaries, where $\beta=\frac{\lambda_s}{\lambda_f}$, and

$$\left.\frac{\partial T_f}{\partial\eta}\right|_{\eta=0}=0,\quad \left.\frac{\partial T_s}{\partial\eta}\right|_{\eta=\frac{1}{\varepsilon}}=0,\tag{20}$$

for symmetric boundaries.

Now write temperatures T_f and T_s as asymptotic expansions in powers of the free parameter σ,

$$T_f=T_{f0}+T_{f1}\sigma+T_{f2}\sigma^2+T_{f3}\sigma^3+\cdots,\tag{21}$$

$$T_s=T_{s0}+T_{s1}\sigma+T_{s2}\sigma^2+T_{s3}\sigma^3+\cdots,\tag{22}$$

where $T_f, T_s, T_{f0}, T_{s0}, T_{f1}, T_{s1}, \ldots$ are each functions of ξ, η, ω_1 and ω_2. The expansions converge rapidly as the value of σ is small.

Upon substituting Eqs. (21) and (22) into Eqs. (17) and (18), we collect terms in like powers of σ, and this leads to a hierarchy of linear differential equation sets. Since σ is a free parameter, the boundary conditions must be satisfied at each power of σ.

At level σ^0:

$$\begin{cases}\frac{\partial^2 T_{f0}}{\partial\eta^2}=0\quad\text{for } 0\leqslant\eta\leqslant1,\\ \frac{\partial^2 T_{s0}}{\partial\eta^2}=0\quad\text{for } 1\leqslant\eta\leqslant\frac{1}{\varepsilon},\\ T_{s0}|_{\eta=1}=T_{f0}|_{\eta=1},\quad \left.\frac{\partial T_{f0}}{\partial\eta}\right|_{\eta=1}=\beta\left.\frac{\partial T_{s0}}{\partial\eta}\right|_{\eta=1},\\ \left.\frac{\partial T_{f0}}{\partial\eta}\right|_{\eta=0}=0,\quad \left.\frac{\partial T_{s0}}{\partial\eta}\right|_{\eta=\frac{1}{\varepsilon}}=0.\end{cases}$$

At level σ^1:

$$\begin{cases}\frac{\partial^2 T_{f1}}{\partial\eta^2}-\frac{Pe}{2}\frac{\partial T_{f0}}{\partial\omega_1}-\frac{3Pe}{4}(1-\eta^2)\frac{\partial T_{f0}}{\partial\xi}=0\quad\text{for } 0\leqslant\eta\leqslant1,\\ \frac{\partial^2 T_{s1}}{\partial\eta^2}-\frac{Pe}{2\phi}\frac{\partial T_{s0}}{\partial\omega_1}=0\quad\text{for } 1\leqslant\eta\leqslant\frac{1}{\varepsilon},\\ T_{s1}|_{\eta=1}=T_{f1}|_{\eta=1},\quad \left.\frac{\partial T_{f1}}{\partial\eta}\right|_{\eta=1}=\beta\left.\frac{\partial T_{s1}}{\partial\eta}\right|_{\eta=1},\\ \left.\frac{\partial T_{f1}}{\partial\eta}\right|_{\eta=0}=0,\quad \left.\frac{\partial T_{s1}}{\partial\eta}\right|_{\eta=\frac{1}{\varepsilon}}=0.\end{cases}$$

At level σ^2:

$$\begin{cases}\frac{\partial^2 T_{f2}}{\partial\eta^2}-\frac{Pe}{2}\frac{\partial T_{f1}}{\partial\omega_1}-\frac{3Pe}{4}(1-\eta^2)\frac{\partial T_{f1}}{\partial\xi}-\frac{\partial T_{f0}}{\partial\omega_2}+\frac{\partial^2 T_{f0}}{\partial\xi^2}=0\quad\text{for } 0\leqslant\eta\leqslant1,\\ \frac{\partial^2 T_{s2}}{\partial\eta^2}-\frac{Pe}{2\phi}\frac{\partial T_{s1}}{\partial\omega_1}-\frac{1}{\phi}\frac{\partial T_{s0}}{\partial\omega_2}+\frac{\partial^2 T_{s0}}{\partial\xi^2}=0\quad\text{for } 1\leqslant\eta\leqslant\frac{1}{\varepsilon},\\ T_{s2}|_{\eta=1}=T_{f2}|_{\eta=1},\quad \left.\frac{\partial T_{f2}}{\partial\eta}\right|_{\eta=1}=\beta\left.\frac{\partial T_{s2}}{\partial\eta}\right|_{\eta=1},\\ \left.\frac{\partial T_{f2}}{\partial\eta}\right|_{\eta=0}=0,\quad \left.\frac{\partial T_{s2}}{\partial\eta}\right|_{\eta=\frac{1}{\varepsilon}}=0.\end{cases}$$

At level σ^3

$$\begin{cases}\frac{\partial^2 T_{f3}}{\partial\eta^2}-\frac{Pe}{2}\frac{\partial T_{f2}}{\partial\omega_1}-\frac{3Pe}{4}(1-\eta^2)\frac{\partial T_{f2}}{\partial\xi}-\frac{\partial T_{f1}}{\partial\omega_2}+\frac{\partial^2 T_{f1}}{\partial\xi^2}=0\quad\text{for } 0\leqslant\eta\leqslant1,\\ \frac{\partial^2 T_{s3}}{\partial\eta^2}-\frac{Pe}{2\phi}\frac{\partial T_{s2}}{\partial\omega_1}-\frac{1}{\phi}\frac{\partial T_{s1}}{\partial\omega_2}+\frac{\partial^2 T_{s1}}{\partial\xi^2}=0\quad\text{for } 1\leqslant\eta\leqslant\frac{1}{\varepsilon},\\ T_{s3}|_{\eta=1}=T_{f3}|_{\eta=1},\quad \left.\frac{\partial T_{f3}}{\partial\eta}\right|_{\eta=1}=\beta\left.\frac{\partial T_{s3}}{\partial\eta}\right|_{\eta=1},\\ \left.\frac{\partial T_{f3}}{\partial\eta}\right|_{\eta=0}=0,\quad \left.\frac{\partial T_{s3}}{\partial\eta}\right|_{\eta=\frac{1}{\varepsilon}}=0.\end{cases}$$

To solve the original set of equations, Eqs. (17)–(20), we must solve the above hierarchy of sets of equations, level by level. The solution at level σ^0 is:

$$T_{f0}\equiv T_{s0}=F_0(\omega_1,\omega_2,\xi),\tag{23}$$

in terms of an unknown function $F_0(\omega_1,\omega_2,\xi)$. Thus, T_{f0} and T_{s0} are equal and independent of the coordinate η.

Making use of Eq. (23), we next solve the equation set at level σ^1:

$$T_{f1}=\frac{Pe(\beta-\beta\varepsilon+\phi\varepsilon)}{16\phi\varepsilon}\frac{\partial F_0}{\partial\omega_1}\eta^4-\frac{Pe(3\beta-3\beta\varepsilon+\phi\varepsilon)}{8\phi\varepsilon}\frac{\partial F_0}{\partial\omega_1}\eta^2+F_1(\omega_1,\omega_2,\xi),\tag{24}$$

$$T_{s1}=\frac{Pe}{4\phi}\frac{\partial F_0}{\partial\omega_1}\eta^2-\frac{Pe}{2\phi\varepsilon}\frac{\partial F_0}{\partial\omega_1}\eta+F_1(\omega_1,\omega_2,\xi)+\frac{Pe(8-5\beta+5\beta\varepsilon-4\varepsilon-\phi\varepsilon)}{16\phi\varepsilon}\frac{\partial F_0}{\partial\omega_1},\tag{25}$$

in terms of some unknown function F_1 which is independent of η. Upon repeating the above procedure, we obtain more complicated results involving unknown functions $F_2(\omega_1,\omega_2,\xi)$, $F_3(\omega_1,\omega_2,\xi),\ldots$ A knowledge of the initial condition and the boundary conditions at the entrance of the system is required in order to determine these functions. Although they are not explicitly known at this stage of the analysis, these functions are known to be independent of η. Therefore, upon treating the η-free functions $F_0, F_1, F_2, \ldots$ as parameters, the dependence of $T_{f0}, T_{f1}, T_{f2}, \ldots$ and $T_{s0}, T_{s1}, T_{s2}, \ldots$ upon η is known.

Fortunately, the relative effective dispersivity can be evaluated from only the incomplete solutions at levels σ^0 and σ^1, owing to the rapid convergence of the expansions in Eqs. (21) and (22) with respect to σ.

Substitution of Eq. (1) into Eq. (14) leads to:

$$\frac{\alpha_{eff}}{\alpha_f}=1+\frac{\varepsilon Pe}{4}\frac{3\int_0^1\eta^2T_f d\eta-\int_0^1T_f d\eta}{\sigma\frac{\partial}{\partial\xi}\int_0^1T_f d\eta}.\tag{26}$$

and upon making use of Eqs. (21) and (26), we obtain:

$$\frac{\alpha_{eff}}{\alpha_f}=1+\frac{\varepsilon Pe}{4}\frac{\frac{Pe(-9\beta+9\beta\varepsilon-2\phi\varepsilon)}{105\phi\varepsilon}\frac{\partial F_0}{\partial\omega_1}+O(\sigma)}{\frac{-\beta+\beta\varepsilon-\phi\varepsilon}{\phi\varepsilon}\frac{\partial F_0}{\partial\omega_1}+O(\sigma)},\tag{27}$$

Now, the infinitesimal $O(\sigma)$ can be ignored as $\sigma=\frac{H}{L}$ is small, resulting in:

$$\frac{\alpha_{eff}}{\alpha_f}=1+CPe^2,\tag{28}$$

and (28)

$$C=\frac{\varepsilon}{420}\frac{9\beta-9\beta\varepsilon+2\phi\varepsilon}{\beta-\beta\varepsilon+\phi\varepsilon}=\frac{\varepsilon}{420}\frac{9(1-\varepsilon)\rho_s c_{ps}+2\varepsilon\rho_f c_{pf}}{(1-\varepsilon)\rho_s c_{ps}+\varepsilon\rho_f c_{pf}}.\tag{29}$$

We emphasise that the second term on the right-hand side of Eq. (28) gives the contribution to the effective thermal diffusivity from the thermal dispersion. This is consistent with a previous observation by Kaviany (1995): a Pe^2 relationship exists if an idealized porous medium has an in-line arrangement, whereas for a stagger arrangement or for a randomized porous structure, the power index is closer to unity.

The analytical results of Eqs. (28) and (29) demonstrate that the dispersion effect scales as Pe^2 for the parallel-plate array model with laminar flows, no matter how the thermal disturbance is introduced and how the initial temperature is distributed. The constant C depends upon both the structural porosity ε and upon the

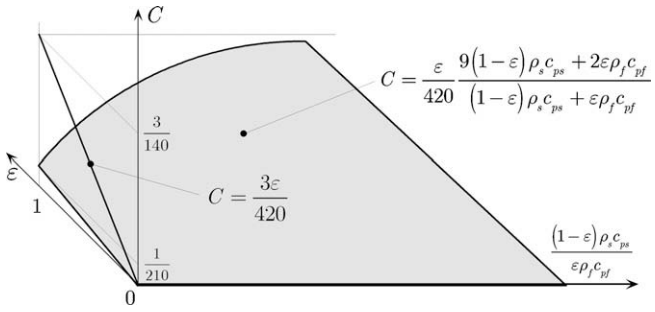

Fig. 4. Coefficient C as a function of porosity ε and effective heat capacity ratio $\frac{(1-\varepsilon)\rho_s c_{ps}}{\varepsilon\rho_f c_{pf}}$. The 3D surface represents coefficient C for transient heat transfer in a general parallel-plate array with a finite plate thickness.

effective heat capacity ratio (defined as the ratio of heat capacity of solid phase to that of fluid phase within unit volume, $\frac{(1-\varepsilon)\rho_s c_{ps}}{\varepsilon\rho_f c_{pf}}$); this dependence is plotted in Fig. 4. In the limit $\varepsilon = 1$ (i.e. the plates have zero thickness), the relative effective dispersivity of (34) reduces to:

$$\frac{\alpha_{eff}}{\alpha_f} = 1 + \frac{1}{210}Pe^2, \tag{30}$$

in agreement with the result given by Kurzweg and Jaeger (1997).

4. Steady heat transfer across an array of parallel plates

Three selected cases are now studied for the steady state transfer of heat occurs across an array of parallel plates and analytical solutions for temperature distributions are obtained:

(1) plates of zero thickness and constant heat flux, q, flowing from plate surfaces into the neighboring fluid channels, illustrated in Fig. 1d;
(2) plates of zero thickness and constant temperature, T_w, at the plate surfaces, illustrated in Fig. 1e;
(3) plates of finite thickness and uniform heat density, $\dot{Q}$, illustrated in Fig. 1c.

4.1. Zero-thickness plate with constant heat flux

If the solid plates have zero thickness (i.e. $D = H$, thus $\varepsilon = 1$), the problem is considerably simplified because the volume averaging is performed on the fluid phase only. Thermal dispersion persists within the array of zero-thickness plates due to the non-uniformity of local fluid velocity.

For this case, the microscopic governing equation for energy in the fluid channel can be written as:

$$\frac{\partial(uT)}{\partial x} = \alpha_f\left(\frac{\partial^2 T}{\partial x^2} + \frac{\partial^2 T}{\partial y^2}\right). \tag{31}$$

Follow the similar y-direction averaging procedure, the macroscopic energy equation becomes:

$$u_{av}\frac{d\langle T\rangle}{dx} = \alpha_{eff}\frac{d^2\langle T\rangle}{dx^2} + \frac{q}{d\rho_f c_{pf}}, \tag{32}$$

where the heat flux arises from the constant heat-flux boundary condition.

Substituting $T = \langle T\rangle + T'$ and $u = \langle u\rangle + u'$ into Eq. (31) and taking the y-direction averaging, we arrive at:

$$u_{av}\frac{d\langle T\rangle}{dx} + \frac{d\langle u'T'\rangle}{dx} = \alpha_f\frac{d^2\langle T\rangle}{dx^2} + \frac{\alpha_f q}{\lambda_f D}. \tag{33}$$

Alternatively, Eq. (33) can be written in a form similar to Eq. (32):

$$u_{av}\frac{d\langle T\rangle}{dx} = \alpha_f\frac{d^2\langle T\rangle}{dx^2} - \frac{d\langle u'T'\rangle}{dx} + \frac{q}{\rho_f c_{pf} D}. \tag{34}$$

Upon comparing Eqs. (32) and (34), we have:

$$\alpha_{eff}\frac{d\langle T\rangle}{dx} = \alpha_f\frac{d\langle T\rangle}{dx} - \langle u'T'\rangle, \quad \text{or} \tag{35}$$

$$\lambda_{eff}\frac{d\langle T\rangle}{dx} = \lambda_f\frac{d\langle T\rangle}{dx} - \rho_f c_{pf}(\langle uT\rangle - \langle u\rangle\langle T\rangle). \tag{36}$$

from which we obtain:

$$\frac{\lambda_{eff}}{\lambda_f} = 1 + \frac{1}{\alpha_f}\frac{\langle u\rangle\langle T\rangle - \langle uT\rangle}{d\langle T\rangle/dx}. \tag{37}$$

The analytical solution for the temperature field in the array is given by (see Appendix B):

$$T = \frac{2q}{\lambda_f Pe}x - \frac{q}{8\lambda_f H^3}y^4 + \frac{3q}{4\lambda_f H}y^2 + T_0, \tag{38}$$

where T_0 is the reference temperature at the origin of the coordinate system. It follows from Eq. (38) that the stream-wise temperature gradient is constant. This gradient is proportional to the heat source density and inversely proportional to the average fluid velocity, fluid heat capacity and distance between plates.

Substitution of Eqs. (1) and (38) into Eq. (37) results in:

$$\frac{\lambda_{eff}}{\lambda_f} = 1 + \frac{3}{140}Pe^2. \tag{39}$$

Again, it is seen that the relative effective dispersivity has the form of $1 + CPe^2$, with $C = \frac{3}{140}$.

4.2. Constant wall-temperature boundary conditions

For zero-thickness plates, we again have $D = H$ and $\varepsilon = 1$. Upon assuming that the solid plates have constant surface temperature, T_w, we obtain the analytical solution for temperature field (see Appendix C):

$$T = T_w - \theta(T_w - T_m) = T_w - \theta\Delta T_0 e^{-\frac{Nux}{PeH}}, \tag{40}$$

where ΔT_0 is the difference between wall temperature and centerline temperature at the entrance, and θ is the dimensionless excess temperature determined from:

$$\frac{d^2\theta}{d\eta^2} + \theta\left(-\frac{3Nu}{4}\eta^2 + \frac{3Nu}{4} + \frac{Nu^2}{Pe^2}\right) = 0. \tag{41}$$

Here, η is the dimensionless coordinate in the cross-stream direction and the associated boundary conditions are given by:

$$\theta|_{\eta=1} = 0, \quad \left.\frac{d\theta}{d\eta}\right|_{\eta=1} = -\frac{Nu}{2}, \quad \left.\frac{d\theta}{d\eta}\right|_{\eta=0} = 0. \tag{42}$$

As discussed in Appendix C, the solution to Eq. (41) subjected to the conditions of (42) is an even function of Pe.

With the above solutions to the temperature field, the effective dispersivity of the parallel-plate array system is given by:

$$\frac{\lambda_{eff}}{\lambda_f} = 1 + Pe^2\frac{1 - \int_0^1 \theta d\eta}{2Nu}. \tag{43}$$

This can be rewritten as $1 + CPe^2$, where

$$C = \frac{1}{2Nu} - \frac{1}{2Nu}\int_0^1 \theta d\eta \tag{44}$$

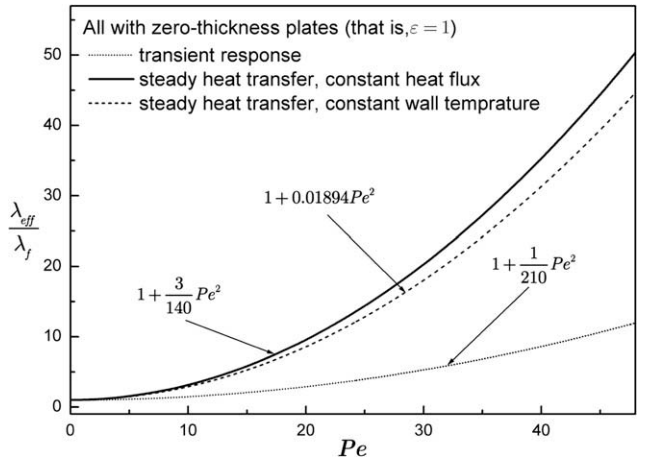

Fig. 5. Relative effective thermal dispersivity as the function of Peclet numbers for zero-thickness plates. Dotted line: for transient heat transfer; solid line: for steady heat transfer with constant heat flux condition; dashed line: for steady heat transfer with constant plate temperature condition.

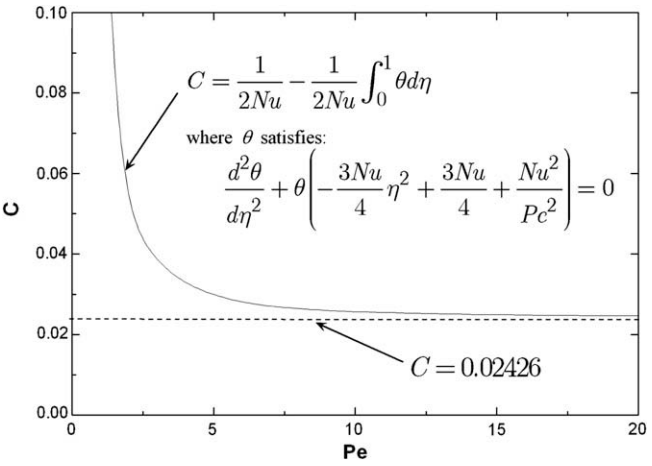

Fig. 6. Coefficient C in Eq. (C21) plotted as a function of Peclet number Pe for constant wall temperature case. As Peclet number Pe increases, coefficient C decreases rapidly and is asymptotic to the constant 0.02426.

depends upon the solution of Eq. (41). Now, Eq. (41) is a non-linear second-order ordinary differential equation, and possesses a closed-form solution (see Appendix C). As the Peclet number Pe is a free variable in Eq. (41), the coefficient C is a function of Pe. Fig. 5 plots the relatively effective dispersivity λ_{eff}/λ_f as a function of Pe, whilst the dependence of C on Pe is shown in Fig. 6. It is seen from these results that the term $\frac{Nu^2}{Pe^2}$ in Eq. (41) is significant only if the Peclet number is relatively small ($Pe < 20$). When $Pe \geqslant 20$, λ_{eff}/λ_f has the usual Pe^2 dependence, and C asymptotes to a constant (Fig. 6).

In order to evaluate the limiting value of C, we ignore the term $\frac{Nu^2}{Pe^2}$ in Eq. (41) to arrive at:

$$\frac{d^2\theta}{d\eta^2} + \theta\left(-\frac{3Nu}{4}\eta^2 + \frac{3Nu}{4}\right) = 0. \tag{45}$$

Solving C from Eqs. (44) and (45), we obtain $C = 0.02426$. Consequently, for usual Peclet numbers ($Pe \geqslant 20$), the relatively effective dispersivity can be written as:

$$\frac{\lambda_{eff}}{\lambda_f} = 1 + 0.02426Pe^2. \tag{46}$$

This limiting value of C is included in Fig. 6.

4.3. Constant heat-flux boundary conditions with finite plate thickness

The final case analysed is an array of parallel plates having finite thickness and uniform heat density $\dot{Q}$. The heat fluxes on all plate surfaces have a single constant value. The situation is similar to that of Case 1 as discussed in Section 4.1 and hence the problem can be solved using the same procedure. With some additional effort, the analytical solution for the temperature field is obtained as:

$$T_f = \frac{(1-\varepsilon)\dot{Q}H}{2\varepsilon Pe\lambda_f}x - \frac{(1-\varepsilon)\dot{Q}}{8\varepsilon\lambda_f H^2}y^4 + \frac{3(1-\varepsilon)\dot{Q}}{4\varepsilon\lambda_f}y^2 + T_0 \quad \text{for } |y| \leqslant H, \tag{47}$$

$$T_s = \frac{(1-\varepsilon)\dot{Q}H}{2\varepsilon Pe\lambda_f}x - \frac{\dot{Q}}{2\lambda_s}y^2 + \frac{\dot{Q}H}{\varepsilon\lambda_s}y + T_0 + \frac{\dot{Q}H^2}{\varepsilon\lambda_s}\left[\frac{5}{8}\beta(1-\varepsilon) - 1 + \frac{\varepsilon}{2}\right] \quad \text{for } H \leqslant |y| \leqslant D, \tag{48}$$

With the above temperature field, the relative effective dispersivity is finally obtained as:

$$\frac{\lambda_{eff}}{\lambda_f} = 1 + \frac{3\varepsilon}{140}Pe^2. \tag{49}$$

The relationship of $1 + CPe^2$ appears again, and $C = \frac{3\varepsilon}{140}$ is independent of Pe.

Note that, when $\varepsilon = 1$, the relationship of (49) reduces to Eq. (39) for an array of parallel plates with zero thickness. In other words, Case 1 as discussed in Section 4.1 is a limiting case of that discussed in this section.

5. Discussion

The analytical results derived above demonstrate that the effective thermal dispersivity of the parallel-plate model depends upon the thermal setting. For each case considered, the thermal dispersion depends only on structure properties and the underlying flow; changes in initial thermal conditions do not change the dispersion. However, the degree of thermal dispersion for the transient case differs from that for the steady state case. And for the steady state case, the magnitude of dispersion is dependent upon the assumed boundary conditions. To illustrate all this, the effective thermal dispersivity is plotted in Fig. 5 as a function of the Peclet number for both steady and transient heat transfer, in limiting case when the solid plates have zero thickness ($\varepsilon = 1$).

For a given Peclet number, the results of Fig. 5 show that the constant wall-temperature boundary condition has the largest dispersion effect whilst the transient case has the smallest effect. This is because:

(i) all three cases have identical velocity non-uniformity;
(ii) for the transient case, the temperature non-uniformity is small as it is caused only by the underlying velocity non-uniformity, and
(iii) for the constant heat flux and constant wall temperature conditions, in addition to the temperature non-uniformity associated with velocity non-uniformity, the imposed heat source condition also contributes to the temperature non-uniformity. Furthermore, the boundary condition of a constant wall temperature enhances the temperature non-uniformity to more than that of the constant heat flux case.

Note that Eq. (28) can be transformed into Eq. (49) when the effective heat capacity ratio $\frac{(1-\varepsilon)\rho_s c_{ps}}{\varepsilon\rho_f c_{pf}}$ becomes infinitely large. This is reasonable by the following reasoning. When the heat capacity of the solid is much larger than that of the fluid, the thermal status of a solid plate is resistant to temperature changes

in the neighboring fluid phase, and hence the heat flux from the solid plate approaches a constant.

6. Conclusions

The analytical results using the parallel-plate array model lead to the following conclusions.

(1) Thermal dispersion in a porous medium such as parallel-plate arrays is caused by the non-uniformity of heat flux distribution at the pore (microscopic) level. This includes both velocity non-uniformity and temperature non-uniformity. Temperature non-uniformity is induced either by velocity non-uniformity or by the thermal boundary conditions.
(2) The effective thermal dispersivity of a porous medium has contributions from both the molecular diffusion and hydraulic dispersion. In the parallel-plate array model, the hydraulic dispersion is always proportional to Pe^2 and quickly surpasses the molecular diffusion as the Peclet number increases, becoming the dominant mechanism for heat transfer.
(3) Thermal dispersion is *not* a property of the porous medium depending only on the pore morphology, porosity and the underlying fluid flow. It is also affected by the type of thermal setting imposed on the medium. This is because the velocity non-uniformity is not the only cause of temperature non-uniformity. The effective thermal dispersivity of a porous medium obtained using one type of thermal setting should be used cautiously when the thermal setting is changed.
(4) Under the condition that the solid heat capacity is much larger than that of the fluid, the case of constant heat source density in solid plates (i.e. the case discussed in Section 4.3) can be represented by the transient case (i.e. that discussed in Section 3). It can be further reduced to the case of constant heat flux when the porosity approaches unity (i.e. the plates have zero thickness, as discussed in Section 4.1).

Acknowledgements

The authors wish to thank the UK Engineering and Physical Sciences Research Council (EPSRC), Overseas Research Students Awards Scheme (ORSAS) and Cambridge Overseas Trust for financial support of this work.

Appendix A. *y*-direction averaging procedure and its characteristics

Recall the *y*-direction averaging procedures as defined in Eqs. (3)–(5). Then, a number of characteristics of volume-averaged variables and useful results can be obtained:

(1) *Averaged variables and deviation variables*:

Volume-averaging is an idempotent operation:

$$\langle\langle\Phi\rangle\rangle = \frac{1}{2D}\int_{-D}^{D}\langle\Phi\rangle dy = \frac{1}{2D}\langle\Phi\rangle 2D = \langle\Phi\rangle,$$

Also,

$$\langle\Phi'\rangle = \frac{1}{2D}\int_{-D}^{D}(\Phi - \langle\Phi\rangle)dy = \frac{1}{2D}\int_{-D}^{D}\Phi dy - \frac{1}{2D}\int_{-D}^{D}\langle\Phi\rangle dy = \langle\Phi\rangle - \langle\Phi\rangle = 0,$$

$$\langle\Phi\rangle' = \langle\Phi\rangle - \langle\langle\Phi\rangle\rangle = \langle\Phi\rangle - \langle\Phi\rangle = 0,$$

$$\Phi'' = \Phi' - \langle\Phi'\rangle = \Phi' - 0 = \Phi'.$$

In summary,

$$\langle\langle\Phi\rangle\rangle = \langle\Phi\rangle, \quad \Phi'' = \Phi' \quad \text{and} \quad \langle\Phi'\rangle = 0, \quad \langle\Phi\rangle' = 0; \tag{A1}$$

(2) Summation and product of two variables:

$$\langle\Phi_1 + \Phi_2\rangle = \frac{1}{2d}\int_{-d}^{d}(\Phi_1 + \Phi_2)dy = \frac{1}{2D}\int_{-D}^{D}\Phi_1 dy + \frac{1}{2D}\int_{-D}^{D}\Phi_2 dy = \langle\Phi_1\rangle + \langle\Phi_2\rangle,$$

$$\begin{aligned}\langle\Phi_1\Phi_2\rangle &= \langle(\langle\Phi_1\rangle + \Phi_1')(\langle\Phi_2\rangle + \Phi_2')\rangle = \langle\langle\Phi_1\rangle\langle\Phi_2\rangle + \Phi_1'\Phi_2' + \langle\Phi_1\rangle\Phi_2' + \Phi_1'\langle\Phi_2\rangle\rangle \\ &= \langle\langle\Phi_1\rangle\langle\Phi_2\rangle\rangle + \langle\Phi_1'\Phi_2'\rangle + \langle\langle\Phi_1\rangle\Phi_2'\rangle + \langle\Phi_1'\langle\Phi_2\rangle\rangle \\ &= \langle\Phi_1\rangle\langle\Phi_2\rangle + \langle\Phi_1'\Phi_2'\rangle + \langle\Phi_1\rangle\langle\Phi_2'\rangle + \langle\Phi_1'\rangle\langle\Phi_2\rangle \\ &= \langle\Phi_1\rangle\langle\Phi_2\rangle + \langle\Phi_1'\Phi_2'\rangle + \langle\Phi_1\rangle 0 + 0\langle\Phi_2\rangle \\ &= \langle\Phi_1\rangle\langle\Phi_2\rangle + \langle\Phi_1'\Phi_2'\rangle\end{aligned}$$

In summary, the volume-averaging operation is linear,

$$\langle\Phi_1 + \Phi_2\rangle = \langle\Phi_1\rangle + \langle\Phi_2\rangle, \quad \langle\Phi_1\Phi_2\rangle = \langle\Phi_1\rangle\langle\Phi_2\rangle + \langle\Phi_1'\Phi_2'\rangle. \tag{A2}$$

(3) *Derivatives*:

$$\begin{aligned}\left\langle\frac{\partial\Phi}{\partial x}\right\rangle &= \frac{1}{2D}\int_{-D}^{D}\frac{\partial\Phi}{\partial x}dy = \frac{1}{2D}\int_{-D}^{D}\lim_{\delta x\to 0}\frac{\Phi(x+\delta x,y)-\Phi(x,y)}{\delta x}dy \\ &= \lim_{\delta x\to 0}\frac{\frac{1}{2D}\int_{-D}^{D}\Phi(x+\delta x,y)dy - \frac{1}{2D}\int_{-D}^{D}\Phi(x,y)dy}{\delta x} \\ &= \frac{\partial}{\partial x}\left(\frac{1}{2D}\int_{-D}^{D}\Phi dy\right) = \frac{\partial\langle\Phi\rangle}{\partial x}.\end{aligned}$$

Similarly,

$$\left\langle\frac{\partial^2\Phi}{\partial x^2}\right\rangle = \frac{\partial}{\partial x}\left\langle\frac{\partial\Phi}{\partial x}\right\rangle = \frac{\partial}{\partial x}\left(\frac{\partial\langle\Phi\rangle}{\partial x}\right) = \frac{\partial^2\langle\Phi\rangle}{\partial x^2}.$$

To summarise, the orders of spatial derivation and volume-averaging are interchangeable,

$$\left\langle\frac{\partial\Phi}{\partial x}\right\rangle = \frac{\partial\langle\Phi\rangle}{\partial x}, \quad \left\langle\frac{\partial^2\Phi}{\partial x^2}\right\rangle = \frac{\partial^2\langle\Phi\rangle}{\partial x^2}. \tag{A3}$$

(4) *Overall volume-averaging and intrinsic volume-averaging*:

$$\langle\Phi\rangle = \varepsilon\langle\Phi\rangle^f = (1-\varepsilon)\langle\Phi\rangle^s, \tag{A4}$$

where $\varepsilon = H/D$ is the porosity of the parallel-plate array.

Appendix B. Analytical solution for constant heat-flux boundary condition

In the fully-developed region for steady heat transfer with a constant input heat flux from the solid phase, the stream-wise temperature gradient and the local heat transfer coefficient are constant along *x*-direction. For the present problem, the local heat transfer coefficient, h_x, along the plate surface is given by Incropera and DeWitt (1985):

$$h_x = \frac{-q}{T_{m,x} - T_{w,x}}, \tag{B1}$$

where $T_{w,x}$ and $T_{m,x}$ are the local values of the plate surface temperature and bulk-mean fluid temperature, respectively. The bulk-mean fluid temperature is defined by Incropera and DeWitt (1985):

$$T_m = \frac{\int_{-H}^{H}(uT)dy}{\int_{-H}^{H}udy}. \tag{B2}$$

Since $h_x = h$ is constant along the x-direction, $T_{m,x} - T_{w,x}$ is also independent of x. This implies that the temperature difference between fluid (bulk-mean) and wall is constant if the wall heat flux is constant and the flow is fully-developed, namely:

$$T_m - T_w = -\frac{q}{h}. \tag{B3}$$

Let the dimensionless excess temperature be defined as the ratio of the difference between a local temperature and the wall temperature to the difference between the bulk-mean temperature and the same wall temperature, all at the same x-position (Incropera and DeWitt, 1985):

$$\theta(x,y) = \frac{T - T_w}{T_m - T_w}, \tag{B4}$$

The boundary conditions can then be written as:

$$\theta|_{y=\pm H} = 0,$$
$$\left.\frac{\partial\theta}{\partial y}\right|_{y=\pm H} = \mp\frac{h}{\lambda_f}.$$

For fully-developed laminar convection, substitution of Eq. (1) into Eq. (B2) leads to:

$$T_m = \frac{3}{4H}\int_{-H}^{H}\left[\left(1 - \frac{y^2}{H^2}\right)T\right]dy. \tag{B5}$$

From Eqs. (B3) and (B4), we have

$$T = -\frac{q}{h}\theta + T_w. \tag{B6}$$

Substituting Eq. (B6) into Eq. (B5), we have

$$T_m = \frac{3q}{4hH}\int_{-H}^{H}\left[\left(1 - \frac{y^2}{H^2}\right)\theta\right]dy + T_w, \tag{B7}$$

and, because of Eq. (B3),

$$\frac{1}{2H}\int_{-H}^{H}\left[\left(1 - \frac{y^2}{H^2}\right)\theta\right]dy = \frac{2}{3}. \tag{B8}$$

Since the right-hand side of Eq. (B8) is a constant, the left-hand side should not depend on x. Hence θ must be independent of x, that is,

$$\frac{\partial\theta}{\partial x} = 0. \tag{B9}$$

Making use of Eqs. (B3), (B6), and (B9), we arrive at:

$$\frac{\partial T}{\partial x} = \frac{dT_m}{dx} = \frac{dT_w}{dx}. \tag{B10}$$

This means that, at any given position along the cross-stream direction, the stream-wise temperature gradient remains unchanged in the stream-wise direction (i.e. $\partial T/\partial x$ does not depend upon y).

Considerations of energy conservation for a volume shown by dashed lines in Fig. 7 lead to:

$$\lambda_f H\frac{d^2T_m}{dx^2} - \rho_f c_{pf} u_m H\frac{dT_m}{dx} = q. \tag{B11}$$

Note that Eq. (B10) has been used to account for the net energy increase due to conduction. Eq. (B11) is a non-homogeneous ordinary linear differential equation of the second order; its general solution is of the form:

$$T_b = C_1 + C_2 e^{\frac{u_m}{\alpha_f}x} + \frac{\alpha_f q}{\lambda_f u_m H}x, \tag{B12}$$

where C_1 and C_2 are constants to be determined, and $\alpha_f = \lambda_f/(\rho_f c_{pf})$.

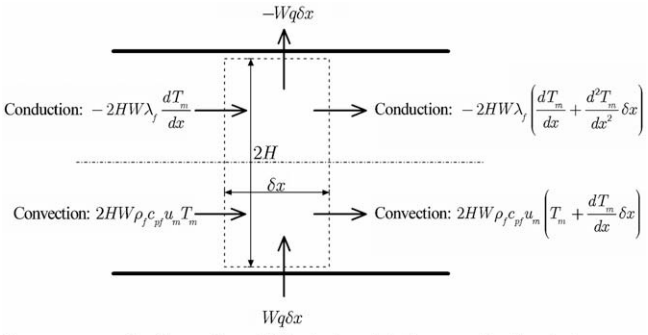

Fig. 7. Energy balance analysis for the case of steady heat transfer (both constant heat flux and constant wall-temperature boundary conditions).

The net energy increase due to stream-wise conduction can be written as:

$$E_{cond} = \lambda_f H\frac{d^2T_m}{dx^2} = C_2\lambda_f H\frac{u_m^2}{\alpha_f^2}e^{\frac{u_m}{\alpha_f}x}, \tag{B13}$$

and that due to convection is given by:

$$E_{conv} = -\rho_f c_{pf} u_m H\frac{dT_m}{dx} = -C_2\lambda_f H\frac{u_m^2}{\alpha_f^2}e^{\frac{u_m}{\alpha_f}x} - q. \tag{B14}$$

If $C_2 \neq 0$, we have the unrealistic situation that $|E_{cond}| \approx |E_{conv}|$ when x is sufficiently large. Therefore we must have $C_2 = 0$, and Eq. (B12) becomes:

$$T_b = C_1 + \frac{\alpha_f q}{\lambda_f u_m H}x. \tag{B15}$$

from which:

$$\frac{d\langle T\rangle}{dx} = \frac{\alpha_f q}{\lambda_f u_m H} = \frac{q}{\rho_f c_{pf} u_m H} = \frac{2q}{\lambda_f Pe}. \tag{B16}$$

This means that the stream-wise temperature gradient $d\langle T\rangle/dx$ is constant in the fully-developed region. The gradient is proportional to the heat source density of plates and inversely proportional to the average fluid velocity, the fluid heat capacity and to the spacing of the plates.

Eqs. (B10) and (B16) suggest that the distribution of temperature in the channel has the form:

$$T = \frac{2q}{\lambda_f Pe}x + f(y). \tag{B17}$$

Substitution of Eq. (B17) into Eq. (3) and the use of Eq. (1) for velocity lead to a second-order ordinary differential equation for the function $f(y)$:

$$\frac{d^2f(y)}{dy^2} = \frac{3q}{2\lambda_f H}\left(1 - \frac{y^2}{H^2}\right). \tag{B18}$$

from which:

$$f(y) = -\frac{q}{8\lambda_f H^3}y^4 + \frac{3q}{4\lambda_f H}y^2 + C_3 y + C_4. \tag{B19}$$

Due to symmetry in the y-direction, $C_3 = 0$, thus:

$$f(y) = -\frac{q}{8\lambda_f H^3}y^4 + \frac{3q}{4\lambda_f H}y^2 + C_4. \tag{B20}$$

Finally, the temperature field in the parallel-plate array system is obtained as:

$$T = \frac{2q}{\lambda_f Pe}x - \frac{q}{8\lambda_f H^3}y^4 + \frac{3q}{4\lambda_f H}y^2 + C_4, \tag{B21}$$

where C_4 is a constant, and can be determined if the temperature at a given location is given. It can be checked that Eq. (B21) satisfies the governing equation and the boundary conditions.

Appendix C. Analytical solution for constant wall-temperature boundary conditions

Under constant wall-temperature boundary conditions, in the fully-developed region for heat transfer, the local heat transfer coefficient, defined by Eq. (B1), and the stream-wise gradient of the dimensionless excess temperature, defined by Eq. (B4), are all constant. By energy conservation of the volume shown in Fig. 7:

$$h(T_w - T_m)dx = \rho_f c_{pf} u_m H dT_m = -\rho_f c_{pf} u_m H d(T_w - T_m) \tag{C1}$$

from which:

$$\frac{d(T_w - T_m)}{(T_w - T_m)} = -\frac{h}{\rho_f c_{pf} u_m H} dx. \tag{C2}$$

If follows immediately that:

$$(T_w - T_m) = C_5 e^{-\frac{h}{\rho_f c_{pf} u_m H} x}, \tag{C3}$$

where the constant C_5 can be determined from the inlet condition (i.e., at $x = 0$), $T_w - T_{m,inlet} = \Delta T_0$. Eq. (C3) can be written as:

$$(T_w - T_m) = \Delta T_0 e^{-\frac{h}{\rho_f c_{pf} u_m H} x}. \tag{C4}$$

Because of Eq. (B4), we have:

$$T = T_w - \theta(T_w - T_m) = T_w - \theta \Delta T_0 e^{-\frac{h}{\rho_f c_{pf} u_m H} x}. \tag{C5}$$

where only θ is a function of the y-coordinate. Substitution of Eq. (C5) into Eq. (31) results in:

$$\frac{d^2\theta}{dy^2} + \theta\left(-\frac{3h}{2\lambda_f H^3} y^2 + \frac{3h}{2\lambda_f H} + \frac{h^2}{\rho_f^2 c_{pf}^2 u_m^2 H^2}\right) = 0. \tag{C6}$$

Introducing the dimensionless coordinate as $\eta = \frac{y}{H}$ and remembering the definitions of Pe and Nu, we can rewrite Eq. (C6) as:

$$\frac{d^2\theta}{d\eta^2} + \theta\left(-\frac{3Nu}{4}\eta^2 + \frac{3Nu}{4} + \frac{Nu^2}{Pe^2}\right) = 0. \tag{C7}$$

Eq. (C7) is a linear second-order ordinary differential equation, with the Nusselt number Nu and Peclet number Pe appearing as parameters. If we can find the solution of Eq. (C7), we can determine the temperature field with Eq. (C5) and then evaluate thermal dispersion for constant wall-temperature boundary conditions.

It can be shown that Eq. (B8) is also satisfied for constant wall-temperature boundary conditions. Eq. (B8) can be written as:

$$\int_0^1 [(1 - \eta^2)\theta] d\eta = \frac{2}{3}. \tag{C8}$$

The solution $\theta(\eta)$ of Eq. (C7) must also satisfy (C8). In addition, it should satisfy the boundary condition:

$$\theta|_{\eta=1} = 0. \tag{C9}$$

Furthermore, $\theta(\eta)$ must be an even function, i.e.:

$$\left.\frac{d\theta}{d\eta}\right|_{\eta=0} = 0, \tag{C10}$$

Finally, by definition, $\theta(\eta)$ must satisfy:

$$\left.\frac{d\theta}{d\eta}\right|_{\eta=1} = -\frac{Nu}{2}. \tag{C11}$$

Eq. (C7) has the form of the well-known Weber Differential Equations (2004). With the introduction of a new dimensionless variable $\zeta = \frac{1}{\sqrt[4]{3Nu}}\eta$, Eq. (C7) can be transformed to a standard form (Parabolic Cylinder Functions, 2004), as:

$$\frac{d^2\theta}{d\zeta^2} - \theta\left(\frac{1}{4}\zeta^2 + p\right) = 0, \tag{C12}$$

where

$$p = -\frac{\sqrt{3Nu}}{4} - \frac{\sqrt{Nu^3/3}}{Pe^2} < 0. \tag{C13}$$

The fundamental solutions to Eq. (C12) are the parabolic cylinder functions given below (Abramowitz et al., 1964):

$$\theta_1(\zeta) = e^{-\frac{\zeta^2}{4}} M\left(\frac{p}{2} + \frac{1}{4}, \frac{1}{2}; \frac{\zeta^2}{2}\right), \tag{C14a}$$

$$\theta_2(\zeta) = \zeta e^{-\frac{\zeta^2}{4}} M\left(\frac{p}{2} + \frac{3}{4}, \frac{3}{2}; \frac{\zeta^2}{2}\right), \tag{C14b}$$

where $M(a, b; x)$ is the Kummer's function of x with regard to parameters a and b (Abramowitz et al., 1964); θ_1 is an even function and θ_2 is an odd function. The general solution to Eq. (C12) is the linear combination of θ_1 and θ_2, $\theta = C_6\theta_1 + C_7\theta_2$. The integral constants, C_6 and C_7, are to be determined by the restriction conditions.

Firstly, $\theta(\zeta)$ remains as an even function after transformation from $\theta(\eta)$, and hence $C_7 = 0$, resulting in $\theta = C_6\theta_1$. With the integral constant C_6 renamed as A, the solution to Eq. (C7) is given by:

Table 1
Values of Nu, A and C for constant wall temperature case and selected values of Pe.

0.001	0.00157	1.29217	56.4032
0.01	0.0156	1.29268	5.63193
0.1	0.154	1.29370	0.578312
1.0	1.28	1.30220	0.702821
2.5	2.39	1.31048	0.380056
5.0	3.17	1.31597	0.0288198
7.5	3.46	1.31820	0.0264768
10.0	3.59	1.31932	0.0255592
15.0	3.69	1.31964	0.0248555
20.0	3.74	1.32015	0.0246123
30.0	3.77	1.32034	0.0244278
75.0	3.78	1.32044	0.0242925
750.0	3.78	1.32069	0.0242653

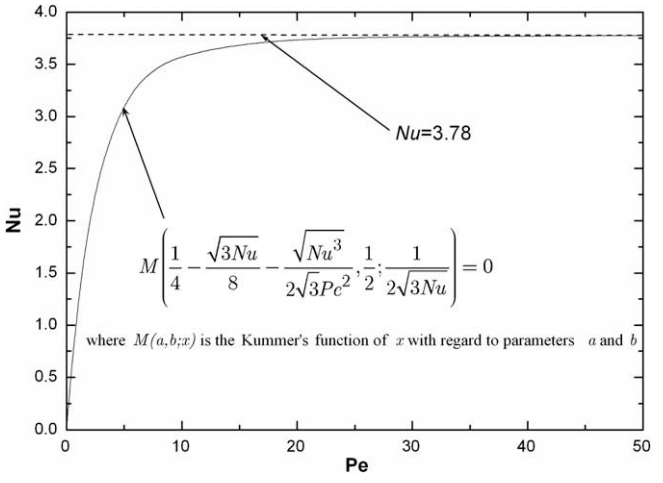

Fig. 8. Nusselt number Nu determined by Eq. (C16) plotted as a function of Peclet number for constant wall temperature case. As Peclet number Pe increases, Nusselt number Nu increases quickly and becomes asymptotic to constant 3.78.

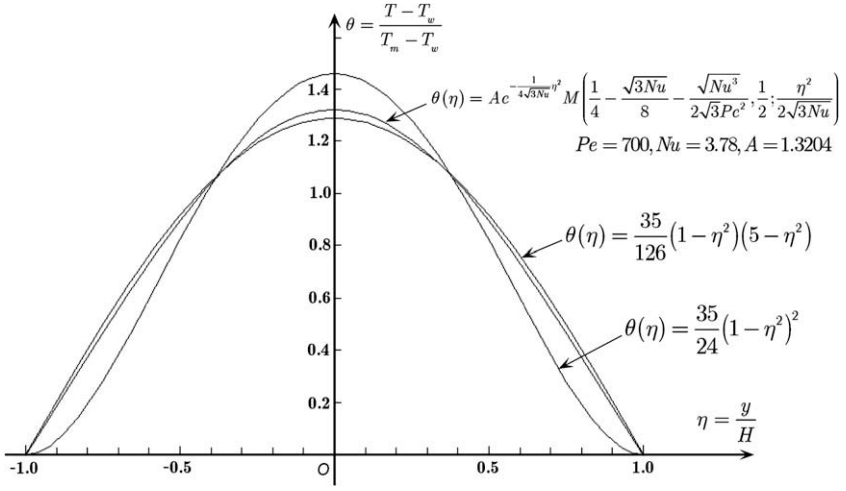

Fig. 9. Dimensionless temperature θ plotted as a function of transverse coordinate η. For transient heat transfer, $\theta(\eta) = \frac{35}{24}(1-\eta^2)^2$, $\theta|_{\eta=0} = 1.4583$, $\langle\theta\rangle = 0.7778$; for steady heat transfer with constant heat flux condition, $\theta(\eta) = \frac{35}{136}(1-\eta^2)(5-\eta^2)$, $\theta|_{\eta=0} = 1.2868$, $\langle\theta\rangle = 0.8235$; for steady heat transfer with constant wall temperature condition, $\theta(\eta) = Ae^{-\frac{1}{4\sqrt{3}Nu}\eta^2} M(\frac{1}{4} - \frac{\sqrt{3}Nu}{8} - \frac{\sqrt{Nu^3}}{2\sqrt{3}Pe^2}, \frac{1}{2}; \frac{\eta^2}{2\sqrt{3}Nu})$ where $Pe = 700$, $Nu = 3.78$, $A = 1.3204$ and $\theta|_{\eta=0} = 1.3204$, $\langle\theta\rangle = 0.8166$.

$$\theta(\eta) = Ae^{-\frac{1}{4\sqrt{3}Nu}\eta^2} M\left(\frac{1}{4} - \frac{\sqrt{3}Nu}{8} - \frac{\sqrt{Nu^3}}{2\sqrt{3}Pe^2}, \frac{1}{2}; \frac{\eta^2}{2\sqrt{3}Nu}\right). \tag{C15}$$

From Eq. (C9), we have:

$$M\left(\frac{1}{4} - \frac{\sqrt{3}Nu}{8} - \frac{\sqrt{Nu^3}}{2\sqrt{3}Pe^2}, \frac{1}{2}; \frac{1}{2\sqrt{3}Nu}\right) = 0. \tag{C16}$$

If the Peclet number Pe is taken as a free parameter, (C16) suggests that the Nusselt number Nu is dependent upon Pe. For selected values of Pe, (C16) can be solved numerically. The solutions are listed in Table 1 and plotted in Fig. 8 as functions of Pe. Note that Nu approaches asymptotically the limit 3.78 as Pe is increased.

Next, the integral constant A is determined with Eq. (C8); the result is listed in Table 1 for different values of Pe. To emphasise the fact that both A and parameter Nu are dependent on Pe, the solution $\theta(\eta)$ is written as:

$$\theta(\eta) = A(Pe)e^{-\frac{1}{4\sqrt{3}Nu(Pe)}\eta^2} M\left(\frac{1}{4} - \frac{\sqrt{3}Nu(Pe)}{8} - \frac{\sqrt{(Nu(Pe))^3}}{2\sqrt{3}Pe^2}, \frac{1}{2}; \frac{\eta^2}{2\sqrt{3}Nu(Pe)}\right). \tag{C17}$$

For $Pe = 75$, we have $Nu = 3.78$, $A = 1.32044$, and the corresponding $\theta(\eta)$ is plotted in Fig. 9. Because $M(a, b; 0) \equiv 1$, A denotes the amplitude factor of the dimensionless excess temperature at the fluid channel centre. For comparison, in Fig. 9, the dimensionless temperature distribution corresponding to other thermal settings is also shown.

To calculate the thermal dispersion we can substitute Eq. (C5) into Eq. (14) to show that the relative effective conductivity is again independent of x-coordinate and is given by:

$$\frac{\lambda_{eff}}{\lambda_f} = 1 + Pe^2 \frac{1}{4Nu} \int_0^1 [(1 - 3\eta^2)\theta] d\eta. \tag{C18}$$

From Eqs. (C8) and (C18), we have:

$$\frac{\lambda_{eff}}{\lambda_f} = 1 + Pe^2 \frac{1 - \int_0^1 \theta d\eta}{2Nu}. \tag{C19}$$

Apparently, the integral $\int_0^1 \theta d\eta$ also depends upon Pe. This is important because, in contrast with the constant heat flux case, we no longer have a simple relationship in the form of $1 + CPe^2$ for the effective thermal diffusivity, as the coefficient C is no longer independent of Pe. To reiterate this, Eq. (C19) is written as:

$$\frac{\lambda_{eff}}{\lambda_f} = 1 + C(Pe)Pe^2, \tag{C20}$$

$$C = \frac{1 - \int_0^1 \theta(Pe; \eta) d\eta}{2Nu(Pe)}. \tag{C21}$$

The value of C is plotted as a function of Pe in Fig. 6.

References

Abramowitz, M., Stegum, I., 1964. Handbook of Mathematical Function with Formulas, Graphs and Mathematical Tables. Reprinted by Dover, New York.

Aris, R., 1956. On the dispersion of a solute in a fluid flowing through a tube. Proc. Roy. Soc. Ser. A (235), 67–77.

Batycky, R.P., Edwards, D.A., Brenner, H., 1993. Thermal Taylor dispersion in an insulated circular cylinder – I. Theory, II. Applications. Int. J. Heat Mass Transfer 36, 4317–4333.

Hsiao, K.T., Advani, S.G., 1999. A theory to describe heat transfer during laminar incompressible flow of a fluid in periodic porous media. Phys. Fluids 11 (7), 1738–1748.

Incropera, F.P., DeWitt, D.P., 1985. Introduction to Heat Transfer. John Wiley & Sons, US.

Kaviany, M., 1995. Principles of Heat Transfer in Porous Media, second ed. Springer.

Kurzweg, G., Jaeger, M.J., 1997. Thermal pulse propagation and dispersion in laminar flow within conduits of finite wall conductivity. Int. J. Heat Mass Transfer 40 (6), 1391–1400.

Kuwahara, F., Nakayama, A., 1999. Numerical determination of thermal dispersion coefficients using a periodic porous structure. ASME J. Heat Transfer 121, 160–163.

Kuwahara, F., Nakayama, A., Koyama, H., 1996. A numerical study of thermal dispersion in porous media. ASME J. Heat Transfer 118, 756–761.

Kuwahara, F., Shirota, M., Nakayama, A., 2001. A numerical study of interfacial convective heat transfer coefficients in two-energy equation model for convection in porous media. Int. J. Heat Mass Transfer 44, 1153–1159.

Mahecha-Botero, A., Grace, J.R., Elnashaie, S.S.E.H., Jim Lim, C., 2007. Time scale analysis of fluidized-bed catalytic reactor based on a generalized dynamic model. In: 2007 ECI Conference on the 12th International Conference on Fluidization – New Horizons in Fluidization Engineering, Vancouver, Canada.

Moyne, C., Didierjean, S., Amaral Souto, H.P., da Silveira, O.T., 2000. Thermal dispersion in porous media: one-equation model. Int. J. Heat Mass Transfer 43, 3853–3867.

Nakayama, A., Kuwahara, F., 1999. A macroscopic turbulence model for flow in a porous medium. J. Fluids Eng. 121, 427–433.

Parabolic Cylinder Functions, June, 2004. <http://mathworld.wolfram.com/ParabolicCylinderFunction.html>.

Quintard, M., Whitaker, S., 1993. Transport in ordered and disordered porous media: volume-averaged equations, closure problems and comparison with experiment. Chem. Eng. Sci. 48, 2537–2564.

Quintard, M., Whitaker, S., 1994. Local thermal equilibrium for transient heat conduction: theory and comparison with numerical experiments. Int. J. Heat Mass Transfer 38, 2779–2796.

Quintard, M., Kaviany, M., Whitaker, S., 1997. Two-medium treatment of heat transfer in porous media: numerical results for effective properties. Adv. Water Resour. 20 (2,3), 77–94.

Taylor, G., 1953. Dispersion of soluble matter in solvent flowing slowly through a tube. Proc. Roy. Soc. Ser. A (219), 86–203.

Taylor, G., 1954. Conditions under which dispersion of a solute in a stream of solvent can be used to measure molecular diffusion. Proc. Roy. Soc. Ser. A (225), 473–477.

Vora, N.P., Contou-Carrere, M.N., Daoutidis, P., 2006. Model reduction of multiple time scale processes in non-standard singularly perturbed form. In: Model Reduction and Coarse-Graining Approaches for Multiscale Phenomena, Springer.

Weber Differential Equations, June, 2004. <http://mathworld.wolfram.com/WeberDifferentialEquations.html>.

Whitaker, S., 1967. Diffusion and dispersion in porous media. AIChE J. 13 (3), 420–427.

Xu, J, 2006. Thermal Dispersion in Wire-Screen Structures, PhD Thesis, University of Cambridge.

Yuan, Z.G., Somerton, W.H., Udell, K.S., 1991. Thermal dispersion in the thick-walled tubes as a model of porous media. Int. J. Heat Mass Transfer 34 (11), 2715–2726.

Zanotti, F., Carbonell, R.G., 1984a. Development of transport equations for multiphase systems – I. General development for two phase systems. Chem. Eng. Sci. 39 (2), 263–278.

Zanotti, F., Carbonell, R.G., 1984b. Development of transport equations for multiphase systems – II. Application to one-dimensional axi-symmetric flows of two phases. Chem. Eng. Sci. 39 (2), 279–297.

Zanotti, F., Carbonell, R.G., 1984c. Development of transport equations for multiphase systems – III. Application to heat transfer in packed beds. Chem. Eng. Sci. 39 (2), 299–311.